A bounding surface model for saturated and unsaturated soil-structure interfaces

Authors: Chao Zhou, Pei Tai* and Jian-Hua Yin

*Corresponding author

Information of the authors

First author: Dr Chao Zhou

Assistant Professor, Department of Civil and Environmental Engineering, The Hong Kong Polytechnic University, Hung Hom, Hong Kong

E-mail: c.zhou@polyu.edu.hk

Corresponding author: Dr Pei Tai

Assistant Professor, School of Civil and Environmental Engineering, Harbin Institute of Technology (Shenzhen), Shenzhen, China

Postdoctoral Fellow, Department of Civil and Environmental Engineering, The Hong Kong Polytechnic University, Hung Hom, Hong Kong

E-mail: pt802@uowmail.edu.au

Co-author: Prof. Jian-Hua Yin

Chair Professor, Department of Civil and Environmental Engineering, The Hong Kong Polytechnic University, Hung Hom, Hong Kong

E-mail: jian-hua.yin@polyu.edu.hk

Abstract

In many geotechnical systems, such as reinforced slopes and embankments, soil-structure interfaces are often unsaturated. Shear behaviour of unsaturated interfaces is strongly dependent on their matric suctions, as revealed by the results of extensive laboratory tests. So far, constitutive models for unsaturated interfaces are very limited in the literature. This paper reports a new bounding surface model for saturated and unsaturated interfaces. New formulations were developed to incorporate suction effects on the flow rule and plastic modulus. To examine the capability of the proposed model, it was applied to simulate suction- and stress-controlled direct shear tests on unsaturated soil-cement, soil-steel and soil-geotextile interfaces. Measured and computed results are well matched, demonstrating that the proposed model can well capture key features of the shear behaviour of unsaturated interfaces, including suction-dependent dilatancy, stress-strain relation, and peak and critical state shear strengths.

Key words: soil-structure interface; unsaturated; suction; dilatancy; critical state

1. Introduction

Shear behaviour of soil-structure interfaces (e.g., shear strength and dilatancy) greatly affects the performance of many geotechnical systems, such as shallow foundations, retaining walls, buried pipelines, landfill covers, concrete-faced rockfill dams, reinforced soil slopes and embankments. Interfaces in these systems are often unsaturated and their matric suctions vary with weather condition. Some researchers investigated the shear behaviour of unsaturated interfaces through suction- and stress-controlled direct shear tests [2,19,21]. They found that, as matric suction increased, the peak and critical state shear strengths increased. The increment of the former was consistently larger than that of the latter, because the dilatancy of soils/interfaces was significantly enhanced by the increase of matric suction [8]. To predict the performance of related geotechnical systems accurately, it is necessary to develop constitutive models suitable for both saturated and unsaturated interfaces.

So far, many constitutive models have been developed for saturated/dry interfaces on the basis of different theoretical frameworks, including classical elastoplasticity [17,28], damage mechanics [22], generalized plasticity [33,34], disturbed state concept [12,13], hyperbolic formulation [9], hypoplasticity [45] and viscoplasticity [42]. Most of these modelling approaches were reviewed by Zhang *et al.* [53] in detail. Readers who are interested in the constitutive modelling of saturated/dry interfaces may refer to these previous studies. The current work focuses on unsaturated interfaces, which have not been given as much attention as saturated/dry interfaces.

Hamid *et al.* [19] proposed a constitutive model for unsaturated interfaces using the

disturbed state concept, which was originally adopted by Desai *et al.* [13] in the modelling of saturated interfaces. The model of Hamid *et al.* [19] was based on two independent stress state variables (i.e., net stress and matric suction). Most of their parameters for modelling mechanical behaviour were functions of matric suction. As a result, extensive tests were required to calibrate their model parameters. Lashkari *et al.* [29] reported a constitutive model for unsaturated interfaces, which was extended from a constitutive model for saturated/dry interfaces [28]. This model adopted the effective (average skeleton) stress and modified matric suction as the constitutive stress variables, similar to the unsaturated soil model of Wheeler *et al.* [52]. In addition, the bonding variable proposed by Gallipoli *et al.* [16] was used as a complementary stress variable to relocate the critical state line (CSL) with the change in matric suction. The model was well verified by the results of 38 tests on seven types of saturated, dry and unsaturated interfaces. Another contribution was made by Lashkari *et al.* [30]. They compared different methods of generalizing a benchmark model [28] for saturated/dry interfaces to consider unsaturated conditions. Particular attention was given to different formulations for the effective stress [24,37] and the CSLs in the unsaturated condition [16,23]. Moreover, three different state indices [1,27,48] were compared. They quantitatively analyzed six different combinations of constitutive equations for the effective stress, CSLs and state indices. In all of these six cases, the measured and computed results are fairly consistent.

In this study, a new constitutive model suitable for both saturated and unsaturated interfaces was developed. Some new formulations were used for describing various aspects of unsaturated interfaces, such as the dilatancy, critical state and plastic modulus. Different from existing

models for unsaturated interfaces, the new model was developed within the bounding surface framework. Compared to the classical elastoplastic framework, it shows some advantages such as the smooth transition between elastic and elastoplastic behaviour, and the capability of modelling cyclic behaviour. Additionally, the proposed model was verified by reported suction-controlled direct shear tests on unsaturated soil-cement, soil-steel and soil-geotextile interfaces.

2. Mathematical formulations

2.1. Constitutive stress variables

With the development of unsaturated soil mechanics, various constitutive stress variables have been proposed based on theoretical and experimental studies. Borja [3] presented a thermodynamically consistent expression for effective stress, in which the Biot coefficient is equal to 1.0, under the assumption of incompressible solid. Later on, Borja [4] extended the theory to the regime of compressible solids. In the new formulation, the Biot coefficient is equal to (1 - K/K_s), where K and K_s are the bulk moduli of soil matrix and solid phase, respectively. The new formulation works for not only soils, but also other porous materials such as rocks and concretes. For soils, the value of K/K_s is usually very small and hence the Biot coefficient can be fixed at 1. Borja *et al.* [5] further incorporated the influence of double porosity by considering the local degrees of saturation and pore fractions. In the current model, the effects of K/K_s and two porosity scales are not considered for simplicity. The following thermodynamically consistent expression is adopted [3]:

$$\begin{Bmatrix} \sigma_n^* \\ \tau \end{Bmatrix} = \begin{Bmatrix} \sigma_{net} + S_r\left(u_a - u_w\right) \\ \tau \end{Bmatrix} \tag{1}$$

where σ_n^* is the effective normal stress at the interface (a positive value means compression); τ is the shear stress at the interface; σ_{net} is the net normal stress at the interface; S_r is the degree of saturation; u_a and u_w are the pore air and water pressures at the interface, respectively. Matric suction s is defined as $(u_a - u_w)$ and it is referred as suction in the following paragraphs for simplicity.

In the unsaturated condition, meniscus water lens are able to increase the normal force at inter-particle contacts without altering the corresponding tangential force, resulting in stabilizing effects on the soils/interfaces [52]. Thus, the apparent preconsolidation pressure of unsaturated soils becomes a function of suction. To model such additional suction effects, the bonding variable ξ proposed by Gallipoli *et al.* [16] is used as a complementary constitutive variable:

$$\xi = f(s)(1 - S_r) \tag{2}$$

where f(s) is a function used to describe the inter-particle normal force (ΔN) imposed by a water meniscus between two identical spherical particles, defined as ΔN at a suction of s normalized by ΔN at zero suction. According to the work of Fisher [14] and Zhou *et al.* [55], $f(s)$ can be readily obtained as follows:

$$f(s) = \frac{3T_s}{Rs} \frac{\left(\sqrt{9 + 8Rs/T_s} - 3\right)\left(\sqrt{9 + 8Rs/T_s} + 1\right)}{16} \tag{3}$$

where T_s is the surface tension coefficient at the air-water interface; R is the radius of spherical particles. This equation suggests that apart from s (suction), R and T_s also affects f(s). The particle size distribution of a soil is generally non-uniform. The median diameter D_{50} is used to

calculate R for simplicity. This simplification should have relatively little impact on the model predictions, because the variation of (1-S_r) is generally much more important than the variation of f(s) in determining the value of ξ in equation (2), as illustrated by Wheeler *et al.* [52]. In addition, the value of T_s does not vary much for the air-water interface, showing only minor variation with temperature. In the temperature range of 20 to 30°C, at which the tests for model verification were carried out, the variation of T_s is less than 2% [38].

When soil becomes fully saturated (S_r = 1), σ_n^* reduces to the effective stress formulation of Terzaghi [46] and ξ is equal to zero. Therefore, the current model allows for a smooth transition between unsaturated and saturated conditions, which is one of the major challenges in the modelling of saturated and unsaturated soils/interfaces [35,54]. It can be used for both saturated and unsaturated interfaces with a single set of parameters.

2.2. Critical state line and state parameter

In a state-dependent constitutive model, the critical state line (CSL) is an important reference state. In the saturated condition, the CSL is a curve in the σ_n^*-τ-e space. Its projections in the σ_n^*-τ and e-lnσ_n^* planes are usually modelled as straight lines:

$$\tau_{cs} = M_s \sigma_n^* \tag{4}$$

$$e_{cs} = \Gamma_s - \omega_s \ln(\frac{\sigma_n^*}{p_{atm}}) \tag{5}$$

where τ_{cs} is the critical state shear strength in the saturated condition; M_s is the critical state stress ratio in the saturated condition; e_{cs} is the critical state void ratio in the saturated condition; Γ_s and ω_s are the intercept and slope of the saturated CSL, respectively.

In the unsaturated condition, the shear strengths of soils and interfaces are both suction-

dependent. The CSL is thus not unique in the plane of mean net stress and deviator stress. Nuth *et al.* [41] analyzed the test data of several soils. They found that in the plane of mean effective stress and deviator stress, the CSLs at various suctions converged remarkably towards the saturated CSL. This finding implies a unique CSL in the plane of mean effective stress and deviator stress, and it has been also echoed by some other researchers based on test data of unsaturated soils and interfaces [30,36]. Thus, the CSLs at various suctions are modelled using a unified formulation:

$$\tau_c = M\sigma_n^* \tag{6}$$

where τ_c is the critical state shear strength; M is the critical state stress ratio independent of suction (i.e., $M = M_s$). Equation (6) works for both saturated and unsaturated conditions.

On the other hand, the critical state void ratio at a given σ_n^* generally becomes larger as soil desaturates. This is because in the unsaturated condition, meniscus water lens are able to stabilize the soil skeleton, as discussed above [52]. By adopting the bonding variable ξ, the unsaturated CSL is linked to the saturated one through the following semi-empirical equation [16]:

$$\frac{e_c}{e_{cs}} = 1 + a\left[\exp(b\xi) - 1\right] \tag{7}$$

where e_c and e_{cs} are the void ratios in unsaturated and saturated conditions at the same σ_n^*, respectively; a and b are model parameters. Based on equations (5) and (7), it is derived that [16]:

$$e_c = \Gamma(\xi) - \omega(\xi)\ln\left(\frac{\sigma_n^*}{p_{atm}}\right) \tag{8}$$

where $\Gamma(\xi)$ and $\omega(\xi)$ are the intercept and slope of the CSL, respectively. Both are dependent on the bonding variable [16]:

$$\begin{cases} \Gamma(\xi) = \Gamma_s \{1 + a[\exp(b\xi) - 1]\} \\ \omega(\xi) = \omega_s \{1 + a[\exp(b\xi) - 1]\} \end{cases} \quad (9)$$

When soil is wetted to saturated conditions, ξ becomes 0 and the values of $\Gamma(\xi)$ and $\omega(\xi)$ are equal to those in the saturated condition. As a result, equations (8) and (9) are applicable for both saturated and unsaturated conditions.

In addition, Figure 1 shows the definition of a state parameter (ψ) proposed by Been *et al.* [1]. It is the difference between the current void ratio (e) and e_c with the same values of σ_n^* and ξ:

$$\psi = e - e_c \quad (10)$$

The values of ψ are positive and negative for interface states on the wet and dry sides of the CSL, respectively.

2.3. Water retention behaviour

The model of Van Genuchten [47] is used to simulate the water retention behaviour of unsaturated soils:

$$S_r = \left[1 + \left(\frac{s}{m_3}\right)^{m_2}\right]^{-m_1} \quad (11)$$

where m_1, m_2 and m_3 are soil parameters. Parameters m_1 and m_2 govern the desorption/ adsorption rate and parameters m_3 is closely related to air-entry value. Equation (11) does not incorporate the influence of void ratio and hydraulic hysteresis for simplicity, considering that

the coupling between hydraulic hysteresis and mechanical behaviour of unsaturated interfaces has not been well studied experimentally. This equation can be further modified, when more experimental evidence is available.

2.4. Elasto-plasticity

The increments of normal and shear strains at the interface are defined as follows:

$$\begin{cases} d\varepsilon_n = \dfrac{du_n}{t} \\ d\varepsilon_t = \dfrac{du_t}{t} \end{cases} \tag{12}$$

where u_n is the normal deformation at the interface (a positive value means contraction); u_t is the tangent displacement at the interface (i.e., the relative displacement between soil and structure); t is the thickness of the interface; $d\varepsilon_n$ is the total increment of normal strain; and $d\varepsilon_t$ is the total increment of shear strain. Variations of the two variables are predicted using the bounding surface plasticity framework, as shown later.

At each loading/unloading process, the incremental/decremental strains consist of elastic and plastic components:

$$\begin{cases} d\varepsilon_n = d\varepsilon_n^e + d\varepsilon_n^p \\ d\varepsilon_t = d\varepsilon_t^e + d\varepsilon_t^p \end{cases} \tag{13}$$

where $d\varepsilon_n^e$ and $d\varepsilon_n^p$ are the elastic and plastic increments of normal strain, respectively; $d\varepsilon_t^e$ and $d\varepsilon_t^p$ are the elastic and plastic increments of shear strain, respectively. For each strain variable, its elastic and plastic components are determined using a decoupled approach.

The elastic strains are calculated as follows:

$$\begin{cases} d\varepsilon_n^e = \dfrac{d\sigma_n^*}{D_n} \\ d\varepsilon_t^e = \dfrac{d\tau}{D_t} \end{cases} \tag{14}$$

where D_n and D_t are the elastic normal and tangent moduli for the interface, respectively.

The plastic strains are expressed as:

$$\begin{cases} d\varepsilon_n^p = \Lambda_t d_t \\ d\varepsilon_t^p = \Lambda_t \end{cases} \tag{15}$$

where Λ_t is the loading index associated with shearing. It is determined by using the condition of consistency and the hardening law. Parameter d_t is the dilatancy defined as the ratio of plastic normal strain to plastic shear strain during the shearing process, and it is obtained from the flow rule. Note that equation (15) is based on two assumptions: (1) the plastic normal and shear strains under constant stress ratio compression are assumed to be zero; (2) the plastic normal and shear strains upon drying/wetting is indirectly considered by the shearing mechanism, which is associated with a change in τ/σ_n^* and/or a change in the bonding variable ξ. The above assumptions keep the model simple and minimize the number of soil parameters, while it is still able to well capture key features of the shear behaviour of an unsaturated interface, as shown later.

2.5. Elastic moduli

According to equation (14), two stiffness parameters (D_n, and D_t) are required to compute the incremental elastic strains. Similar to the model of Liu *et al.* [33] for saturated interfaces, the stiffness parameters D_n and D_t are calculated using the following formulations [26]:

$$D_t = D_{t0}\frac{1+e}{e}\left[\left(\frac{\sigma_n^*}{p_{atm}}\right)^2 + R\left(\frac{\tau}{p_{atm}}\right)^2\right]^{0.5} \tag{16}$$

$$D_n = D_t\, R \tag{17}$$

where D_{t0} is a parameter depending on the inherent property of an interface; R is the ratio of elastic normal modulus to elastic shear modulus. According to some previous studies on unsaturated soils, the elastic moduli are significantly affected by suction [39,40]. Equations (16) and (17) assume that suction is able to affect the elastic moduli of an interface by increasing the effective normal stress.

2.6. Bounding and yield surfaces

As summarized and illustrated by Dafalias [10], the main feature of bounding surface models is the dependency of plastic modulus on the distance between actual and "imaged" stress states. In addition to this main feature, each bounding surface model has some special features regarding the definition and description of bounding surface. The current model adopts the approach of Wang *et al.* [50]. Two bounding surfaces are defined in the $\sigma_n^* - \tau$ plane, as shown in Figure 2. The first one is the maximum prestress memory bounding surface, described as

$$F_t = \tau - M_m\sigma_n^* \tag{18}$$

where M_m is the maximum stress ratio of the interface in the stress history. During primary shearing, the bounding surface F_t rotates about point O with the size controlled by M_m. During other loading/unloading paths, the bounding surface F_t does not change if the stress state has not reached the bounding surface.

The other one is the so-called failure bounding surface, which is mathematically defined as

$$\overline{F}_t = \tau - M_b \sigma_n^* \tag{19}$$

$$M_b = M \exp(-n_b \psi) \tag{20}$$

where M_b is the attainable peak stress ratio (failure stress ratio) [11]; n_b is a positive model parameter. The value of M_b depends on the current value of state parameter ψ. When ψ is positive and negative, M_b is below and above M, respectively. Different from the first bounding surface, the location of this bounding surface is affected by the loading/unloading inside it, because cyclic loading/unloading would induce a change in ψ.

The above two bounding surfaces are both used in the determination of loading index. The condition of consistency is imposed on the bounding surface F_t during primary shearing, as shown later. Note that this modelling approach has been used in many constitutive models for soils (e.g., [18,31,49]). The monotonic and cyclic shear behaviour of soils can be well captured by these previous models, suggesting that this modelling approach is efficient.

In addition, a yield surface is defined in the $\sigma_n^* - \tau$ plane using the following equation [11,15]:

$$f_t = \left| \frac{\tau}{\sigma_n^*} - \alpha \right| - m \tag{21}$$

where α is a stress ratio depending on the stress history; m is a soil parameter. Equation (21) defines a "wedge", which is the elastic threshold of an interface subjected to shearing. The size and location of this wedge are governed by *m* and α, respectively. Following Dafalias *et al.* [11], a constant value of 0.01 is used for m in this study, meaning that the size of the elastic zone does not change. This simplification barely has any notable effect on the model prediction,

particularly in the range of large strains where stress state is on this yield surface. In addition, the evolution of this yield surface is described by the kinematic hardening law. When the stress state is on the wedge and shearing continues (i.e., $d\eta > 0$ and $d\eta < 0$ at the upper and lower wedge lines, respectively, where $d\eta$ is the change of stress ratio), soil behaviour is elastoplastic. Meanwhile, α changes to ensure that stress state remains on the yield surface (i.e., condition of consistency). Hence, $d\alpha$ should be equal to $d\eta$ under the assumption of constant m [11]. For other cases, the interface behaviour is elastic and α maintains constant.

2.7. Mapping rule

Mapping rule is a very important component in bounding surface models. It is used to project the actual stress state onto the bounding surface to obtain an "imaged" stress state. The distance between the actual and "imaged" stress states affects different aspects of soil behaviour, such as the plastic modulus. The current model adopts a mapping rule originally proposed by Li [31] for saturated soils. The reverse stress ratio η_r, corresponding to the stress ratio at which there was the last change in the direction of shearing (i.e., the sign of $d\eta$ changed), serves as the projection center. The variable M_m is the "imaged" stress ratio. Based on this mapping rule (see Figure 2), two Euclidian "distances" (ρ_t and $\bar{\rho}_t$) are defined:

$$\rho_t = \eta - \eta_r \tag{22}$$

$$\bar{\rho}_t = M_m - \eta_r \tag{23}$$

where η is the current stress ratio τ/σ_n^*; The ratio of these two Euclidian "distances" ($\rho_t/\bar{\rho}_t$) is often used to model the influence of stress history on the dilatancy and plastic modulus [11]. The value of $\rho_t/\bar{\rho}_t$ is very small immediately after changing the direction of shearing. Upon

subsequent shearing in the same direction, the value of $\rho_t/\bar{\rho}_t$ continuously increases until 1, when η becomes equal to M_m.

In addition, it should be pointed out that according to this mapping rule, small fluctuations of stress during shear reversal would require an update of η_r and therefore induce numerical errors. To avoid this problem, η_r is not immediately updated upon stress reversal. The update is made only when soil stress state reaches the yield surface, where $\rho_t/\bar{\rho}_t$ is non-zero. Consequently, numerical errors induced by small fluctuations of stress inside yield surfaces could be effectively eliminated in the proposed model. This is one of the advantages to incorporate the yield surface even though a constant and small *m* is used.

2.8. State-dependent dilatancy

The dilatancy (or flow rule), which corresponds to the variable d_t in equation (15), is a very important aspect of the interface behaviour and boundary value problems. For instance, in pile engineering, the interface dilatancy would affect the normal stress acting on the pile and hence affect shaft resistance of the pile. The dilatancy of an interface can be modelled in a similar approach to that used for soil dilatancy, as illustrated by Liu *et al.* [33].

So far, many formulations have been reported for describing the dilatancy of saturated and unsaturated soils. Li *et al.* [32] developed the theory of state-dependent dilatancy, which was then extended by Chiu *et al.* [8] from saturated to unsaturated conditions. During primary shearing ($\bar{\rho}_t/\rho_t = 1$), the dilatancy is expressed as

$$d_t = \frac{d_0}{M}(M_d - \eta) \tag{24}$$

$$M_d = M \exp(n_d \psi) \tag{25}$$

where d_0 is a soil parameter; n_d is a soil parameter which generally takes a positive value; M_d is the stress ratio at which phase transformation occurs during primary shearing (i.e., on the bounding surface with $\bar{\rho}_t/\rho_t = 1$). If the void ratio decreases (i.e., a larger density), equations (10) and (25) predict a smaller ψ and a lower M_d. Consequently, phase transformation takes place at an earlier stage of shearing.

Following Li [31], for stress path other than primary shearing, equation (24) is modified by incorporating the term $\sqrt{\bar{\rho}_t/\rho_t}$:

$$d_t = \frac{d_0}{M}\left(M_d\sqrt{\frac{\bar{\rho}_t}{\rho_t}} - \eta\right) \tag{26}$$

Equation (26) suggests that at any particular value of η, the value of d_t is greater (more contractive) for stress states inside the bounding surface ($\bar{\rho}_t/\rho_t > 1$) than during primary shearing on the bounding surface ($\bar{\rho}_t/\rho_t = 1$). The incorporation of $\bar{\rho}_t/\rho_t$ can better capture soil behaviour under cyclic shear [31].

2.9. Hardening law

The loading index Λ_t in equation (15) is determined using the condition of consistency and hardening law. As explained in the section 2.6, the condition of consistency is imposed on the bounding surface F_t during primary shearing. Similar to the work of Chiu *et al.* [8], M_m is considered as the hardening parameter, and the hardening of the bounding surface F_t only depends on the plastic volumetric strain due to primary shearing. Under this assumption, during primary shearing, when yielding is occurring with the stress state on the bounding surface F_t, the condition of consistency suggests that

$$\frac{\partial F_t}{\partial \sigma_n^*} d\sigma_n^* + \frac{\partial F_t}{\partial \tau} d\tau + \frac{\partial F_t}{\partial M_m} \frac{\partial M_m}{\partial \varepsilon_n^p} d_t \Lambda_t = 0 \tag{27}$$

Similar to state-dependent models for soils [8,32,55], a plastic modulus (K_t^p) is introduced and defined as follows:

$$K_t^p = -\frac{\partial F_t}{\partial M_m} \frac{\partial M_m}{\partial \varepsilon_n^p} d_t \tag{28}$$

By substituting equation (28) to (27), it follows that, for primary shearing, on the F_t bounding surface

$$\Lambda_t = \frac{1}{K_t^p} \left(\frac{\partial F_t}{\partial \sigma_n^*} d\sigma_n^* + \frac{\partial F_t}{\partial \tau} d\tau \right) = \frac{1}{K_t^p} \left(d\tau - M_m d\sigma_n^* \right) \tag{29}$$

This equation can be used to determine the loading index Λ_t in equation (15). It is clear that for a given stress increment, the value of Λ_t is controlled by the plastic modulus. During primary shearing, a state-dependent plastic modulus is adopted here:

$$K_t^p = \frac{D_t h}{M_m} \left(M_b - M_m \right) \tag{30}$$

where h is a positive model parameter. Note that equations (29) through (30) has been derived solely for primary shearing paths, on the bounding surface. For elastoplastic paths inside the bounding surface, the bounding surface plasticity theory is used. These three equations can also be used for Λ_t, if appropriate adjustment is made for the definition of the plastic modulus K_t^p.

$$K_t^p = \frac{D_t h}{M_m} \left(M_b \left(\frac{\bar{\rho}_t}{\rho_t} \right) - M_m \right) \tag{31}$$

Equation (31) suggests that the value of K_t^p is greater for stress states inside the bounding surface ($\bar{\rho}_t / \rho_t > 1$) than during primary shearing on the bounding surface ($\bar{\rho}_t / \rho_t = 1$). This is

consistent with experimental results that given the same stress increment, the plastic strain is smaller for stress states inside the bounding surface. Moreover, it should be noted that $\sqrt{\bar{\rho}_t/\rho_t}$ and $\bar{\rho}_t/\rho_t$ are used in equations (26) and (31), respectively. This can ensure that the predicted value of $\mathrm{d}\varepsilon_n^p$ is zero when $\bar{\rho}_t/\rho_t$ approaches infinity (i.e., predicting essentially elastic behaviour immediately updating η_r). This is because as $\bar{\rho}_t/\rho_t$ approaches infinity, although d_t predicted by equation (26) tends to approach infinity, it approaches infinity more slowly than the value of K_t^p given by equation (31). In addition, the plastic strain increment is zero for a stress increment remaining inside the yield surfaces, even if the value of K_t^p given by equation (31) is not infinite.

3. Calibration of model parameters

The proposed model has 15 parameters and they are summarized in Table I. Nine of them (D_{t0}, R, M, ω_s, Γ_s, n_d, d_0, n_b, and h) are required for the saturated and dry conditions, while another five parameters (m_1, m_2, m_3, a and b) are used to incorporate unsaturation effects. The last one t is a parameter of interface characteristics. All of these parameters can be calibrated based on suction- and stress-controlled interface tests, as explained in the following paragraphs:

(a). Three parameters are required for the water retention behaviour: m_1, m_2 and m_3 (see equation (11)). These three parameters can be determined by fitting the measured WRC. At least one water retention test should be carried out.

(b). The interface thickness *t* is assumed to be 5 mm in all simulations. Its value does not affect the model prediction much as long as the same value is also used in the calibration of model parameters [33].

(c). According to equations (16) and (17), there are two elastic parameters: D_{t0} and R. Parameter D_{t0} can be calibrated from the measured relationship between shear strain and shear stress at the interface. At the early stage of shearing, the ratio of τ/p_{atm} is small and the plastic strain is almost zero. Hence, equations (14) and (16) suggest that

$$D_{t0} = \frac{d\tau}{d\varepsilon_t} \frac{e}{1+e} \frac{p_{atm}}{\sigma_n^*} \tag{32}$$

Similarly, equations (14) and equation (17) suggest that D_n and hence R can be determined through normal compression test:

$$D_n = \frac{d\sigma_n^*}{d\varepsilon_n} \tag{33}$$

$$R = \frac{D_n}{D_t} \tag{34}$$

It can be seen from equations (32) to (34) that at least two interface tests at either saturated or unsaturated conditions are required to calibrate the elastic parameters, including one shear test and one normal compression test.

(d). The proposed model requires five parameters to define the CSL of an unsaturated interface (i.e., M, ω_s, Γ_s, a, and b), as shown in equations (6) and (9). The first three parameters are obtained from the CSL in the saturated condition, and the calibration of them requires at least two shear tests. M is calibrated from experimental results in the σ_n^*-τ plane, while ω_s and Γ_s are determined from the slope and intercept in the e-lnσ_n^* plane. Parameters a and b are determined by fitting the CSLs in the unsaturated condition using equations (8) and (9), and at least two unsaturated shear tests are needed.

(e). Two parameters (n_d and d_0) (see equations (25) and (26)) are used to define the dilatancy. According to equation (26), when the interface response changes from contraction to dilation under primary shearing (i.e., $\rho_t / \bar{\rho}_t = 1$), η is equal to M_d. Therefore, equation (25) suggests that

$$n_d = \frac{1}{\psi} \ln\left(\frac{\eta}{M}\right) \tag{35}$$

The values of η and ψ corresponding to a point of phase transformation can be obtained from a shear test and then parameter n_d can be calculated using equation (35). After determining n_d, the other dilatancy parameter d_0 can be determined by fitting the measured relationship between dilatancy and stress ratio during primary shearing:

$$d_0 = \frac{M d_t}{(M \exp(n_d \psi) - \eta)} \tag{36}$$

It can be seen from equations (35) and (36) that one primary shear test in either saturated or unsaturated conditions are required to calibrate the two dilatancy parameters.

(f). The plastic modulus requires two parameters (n_b and h in equations (20) and (30)). Based on these equations, when the shear stress reaches the peak value (i.e., $d\tau/d\varepsilon_t=0$ and $M_b = \eta$), parameter n_b can be determined as follows:

$$n_b = -\frac{1}{\psi} \ln\left(\frac{\eta}{M}\right) \tag{37}$$

The other hardening parameter h can be also determined through primary shear tests in constant-σ_n^* condition. Under the assumption that the elastic shear strain is negligible, it is obtained that

$$\frac{d\tau}{d\varepsilon_t} = K_t^p \tag{38}$$

Substituting equations (20) and (30) into equation (38), with primary shearing corresponding to $\rho_t/\bar{\rho}_t = 1$ and $M_m = \eta$, yields:

$$h = \frac{d\tau/d\varepsilon_t}{D_t\left[M\exp(-n_b\psi)/\eta - 1\right]} \tag{39}$$

Parameter h can be obtained by fitting measured stress-strain relationship using equation (39). Equations (37) and (39) suggest that one primary shear test is required to calibrate the two parameters for plastic modulus. This test should be carried out in the saturated and drained condition, so that σ_n^* can be easily maintained constant.

4. Model verification

The proposed model is applied to simulate suction- and stress-controlled direct shear tests on various unsaturated interfaces, including a soil-steel interface [19], a soil-geotextile interface [25] and a soil-cement interface [21]. In addition, to evaluate the model performance for cyclic shear behaviour, a cyclic shear test on a saturated sand-steel interface [43] is also simulated. For each type of interface, the model parameters are calibrated using the above method and summarized in Table I.

4.1. Shear behaviour of an unsaturated soil-steel interface

Hamid *et al.* [19] developed a suction- and stress-controlled direct shear box for studying the shear behaviour of unsaturated soil-structure interfaces. The suction was controlled using the axis-translation technique [20]. They tested a soil-steel interface. The soil (Minco silt) was sampled from central Oklahoma with a median diameter D_{50} of 0.05 mm. The steel plate is 102 mm in diameter and the maximum peak to valley roughness height R_{max} is 0.38 mm. Three

different net normal stresses (105, 140 and 210 kPa) and suctions (20, 50 and 100 kPa) were considered.

Figure 3 shows the measured and computed shear behaviour at a suction of 100 kPa and different net normal stresses of 105, 140 and 210 kPa. For the computed results, values of model parameters are given in Table 1. In all stress conditions, the computed and measured results are well matched. This implies that the model is able to well capture the influence of net stress on the interface shear behaviour. On the other hand, this series of tests were also simulated by some previous researchers [19,29,30]. The predictions of three different models are also shown in Figure 3 and the corresponding parameter values are summarized in Table II. These three models use different constitutive stress variables from the current model: Hamid *et al.* [19] used net stress and suction; Lashkari *et al.* [29] used the effective (average skeleton) stress, modified matric suction, and the bonding variable of Gallipoli *et al.* [16] as a complementary variable; the model II in Lashkari *et al.* [30] adopted the effective stress formulation of Khalili *et al.* [24] and another complementary variable (i.e., the bonding variable of Hu *et al.* [23]). For each model, the measured and computed results are fairly consistent. This analysis suggests that the performances of these models are all satisfactory. Compared with the previous models, less parameters are required in the current model.

Figure 4 compares the measured and computed results at a net normal stress of 105 kPa and different suctions of 20, 50 and 100 kPa. It can be seen from the experimental results that when suction increases from 20 to 100 kPa, the peak shear strength increases by about 50%, while the increase in the critical state shear strength is much smaller (about 10-15%). The different

suction effects on the peak and critical state shear strengths are mainly because the dilatancy is more significant at a higher suction, as confirmed by the measured relations between tangent and normal displacements. Furthermore, the observed suction effects on the dilatancy can be well explained using the proposed model. When suction increases, the critical state line in the $e - ln\sigma_n^*$ plane shifts upwards (i.e., exhibiting a larger void ratio at the same σ_n^*), as shown in equation (9). As a result, the state parameter of the interface in a given stress and void ratio condition becomes lower. The interface is therefore more dilative (see equations (25) and (26)) and shows a larger peak shear strength (see equations (20) and (30)).

4.2. Shear behaviour of an unsaturated soil-geotextile interface

Figure 5 and Figure 6 show the shear behaviour of an unsaturated soil-geotextile interface. The experimental results were reported by Khoury *et al.* [25]. The test soil is non-plastic and has a grain size distribution similar to that of fine sandy silt, with a D_{50} of 0.071 mm. For the geotextile (102 mm in diameter), the maximum peak to valley roughness height R_{max} is 0.3 mm. Three different net normal stresses (50, 100 and 300 kPa) and suctions (20, 50 and 100 kPa) were applied in their tests. Using model parameter values given in Table 1, the computed and measured results are well matched in all stress and suction conditions, demonstrating the good capability of the proposed model in simulating the shear behaviour of the unsaturated soil-geotextile interface.

It should be noted that, at a net stress of 100 kPa, the shear strength of the soil-geotextile interface decreases as suction increases from 50 kPa to 100 kPa (see Figure 5(a)). This observation is different from the behaviour of the soil-steel interface presented in Figure 4.

These two trends are all captured by the proposed model in a unified approach. According to the proposed model, the discrepancy is mainly because the shear behaviour of unsaturated soils and interfaces is affected by not only suction but also degree of saturation [7]. The effective normal stress can either increase or decrease when suction increases (see equation (1)), depending on the desorption rate of the WRC. Therefore, it is important to incorporate both suction and degree of saturation in an unsaturated interface model.

4.3. Shear behaviour of an unsaturated soil-cement interface

Hossain *et al.* [21] investigated the shear behaviour of an unsaturated soil-cement interface using a suction- and stress-controlled direct shear apparatus. The test soil is completely decomposed granite (silty sand) sampled from Hong Kong, with a D_{50} of 0.08 mm. For a square cement surface (100 mm by 100 mm), the maximum peak to valley roughness height R_{max} is 0.8 mm. A suction range of 0 to 100 kPa and a stress range of 50 to 300 kPa were adopted in their studies.

Figure 7 compares the measured and computed shear behaviour at a net normal stress of 100 kPa and different suctions of 0, 50 and 100 kPa, with model parameter values listed in Table 1. Key features of the shear behaviour, such as the increase of dilatancy and peak shear strength with increasing suction, are all well predicted by the new model. This is mainly attributed to the proper consideration of suction effects, as discussed above.

Figure 8 shows the measured and computed shear behaviour at saturated condition. Three levels of effective normal stress are considered: 50, 100 and 300 kPa. The measured results show that as the effective normal stress increases, the interface becomes stronger and more

contractive. This influence of effective normal stress is well captured, mainly attributed to the proper formulations for the critical state shear strength and dilatancy (equation (26)).

4.4. Cyclic shear behaviour of a saturated sand-steel interface

Shahrour *et al.* [43] investigated the behaviour of a saturated sand-steel interface under monotonic and cyclic shearing. Monotonic shear tests were carried out in different conditions of effective normal stress (100, 200 and 300 kPa) and relative compaction (15% and 95%). Cyclic shear tests were carried out at effective normal stress of 100 kPa and relative compaction of 95%. Houston sand with a D_{50} of 0.7 mm was used in the tests, but the value of R_{max} for the steel surface was not reported. As shown in Figure 9, the measured and computed results show great consistency under both monotonic and cyclic shearing. In future studies, the proposed model should be further verified using test data from cyclic shear tests on unsaturated interfaces, which is currently not available in the literature.

The above comparisons demonstrate that the proposed model is able to well capture the behaviour of saturated and unsaturated interfaces. For numerical modelling of boundary value problems, this interface model will be implemented in a finite element code in a further study. In addition, the model of Zhou *et al.* [55] can be used in this code to model soils, which employs equivalent constitutive stress variables and an equivalent modelling approach as the current interface model. The numerical implementation of advanced models for unsaturated soils and interfaces is by no means a simple and trivial task, requiring robust computational algorithms. For instance, some researchers noted the non-convexity of the loading-collapse (LC) yield surface [44,51] along the suction axis. The lack of convexity could result in two problems: (a)

the elastic prediction could overshoot the plastic region on the non-convex side and therefore underestimate the plastic strain; (b) the algorithm could result in a non-unique plastic return mapping because there is more than one normal direction to the yield surface on the non-convex side [3]. The first problem can be readily solved by using a small load increment. More importantly, Borja [3] circumvented the second problems by treating suction as a strain-like variable and determining plastic return map in constant-s condition. The formulations of Borja [3] has been seamlessly implemented by Borja *et al.* [6] using the return mapping algorithm. These constitutive formulations and algorithms would be helpful in future numerical implementations.

5. Summary and conclusions

A new bounding surface model has been developed for describing the elastoplastic behaviour of saturated and unsaturated interfaces. In this paper, the constitutive formulations, calibration of model parameters, as well as model verification are presented and discussed in detail.

To verify the proposed model, it is applied to simulate suction- and stress-controlled direct shear tests on unsaturated soil-cement, soil-steel and soil-geotextile interfaces. Computed and measured results are fairly consistent. The models show good predictions of key features of the shear behaviour of saturated and unsaturated interfaces, including (1) the shear strengths at the critical and peak states are affected by suction; (2) the interface becomes more dilative as suction increases. In addition, as a preliminary attempt, the proposed model is used to model the cyclic shear behaviour of a saturated sand-steel interface. The measured and computed

results are fairly consistent.

6. Acknowledgements

The authors would like to thank the Research Grants Council (RGC) of the HKSAR for providing financial support through the grants 16216116, 16212218 and AoE/E-603/18.

References

1. Been K, Jefferies MG. A state parameter for sands. *Géotechnique* **35**: 99-112, 1985.

2. Borana L, Yin JH, Singh DN, Shukla SK. Interface behavior from suction-controlled direct shear test on completely decomposed granitic soil and steel surfaces. *International Journal of Geomechanics* **16**: D4016008, 2016.

3. Borja RI. Cam-Clay plasticity. Part V: A mathematical framework for three-phase deformation and strain localization analyses of partially saturated porous media. *Computer Methods in Applied Mechanics and Engineering* **193**: 5301-5338, 2004.

4. Borja RI. On the mechanical energy and effective stress in saturated and unsaturated porous continua. *International Journal of Solids and Structures* **43**: 1764-1786, 2006.

5. Borja RI, Koliji A. On the effective stress in unsaturated porous continua with double porosity. *Journal of the Mechanics and Physics of Solids* **57**: 1182-1193, 2009.

6. Borja RI, Song X, Wu W. Critical state plasticity. Part VII: Triggering a shear band in variably saturated porous media. *Computer Methods in Applied Mechanics and Engineering* **261**: 66-82, 2013.

7. Chen R, Ng CWW. Impact of wetting–drying cycles on hydro-mechanical behavior of an unsaturated compacted clay. *Journal of Applied Clay Science* **86**: 38-46, 2013.

8. Chiu CF, Ng CWW. A state-dependent elasto-plastic model for saturated and unsaturated soils. *Geotechnique* **53**: 809-829, 2003.

9. Clough GW, Duncan JM. Finite element analyses of retaining wall behavior. *Journal of Soil*

Mechanics & Foundations Div **12**: 1657-1673, 1971.

10. Dafalias YF. Bounding surface plasticity. I: Mathematical foundation and hypoplasticity. *Journal of Engineering Mechanics* **112**: 966-987, 1986.
11. Dafalias YF, Manzari MT. Simple plasticity sand model accounting for fabric change effects. *J Eng Mech-Asce* **130**: 622-634, 2004.
12. Desai CS. *Mechanics of materials and interfaces: The disturbed state concept*edn: CRC press, 2000.
13. Desai CS, Ma Y. Modelling of joints and interfaces using the disturbed‐state concept. *International Journal for Numerical and Analytical Methods in Geomechanics* **16**: 623-653, 1992.
14. Fisher R. On the capillary forces in an ideal soil; correction of formulae given by WB Haines. *The Journal of Agricultural Science* **16**: 492-505, 1926.
15. Gajo A, Wood M. Severn–Trent sand: a kinematic-hardening constitutive model: the q–p formulation. *Géotechnique* **49**: 595-614, 1999.
16. Gallipoli D, Gens A, Sharma R, Vaunat J. An elasto-plastic model for unsaturated soil incorporating the effects of suction and degree of saturation on mechanical behaviour. *Géotechnique* **53**: 123-135, 2003.
17. Ghionna V, Mortara G. An elastoplastic model for sand–structure interface behaviour. *Géotechnique* **52**: 41-50, 2002.
18. Gu Q, Wang G. Direct differentiation method for response sensitivity analysis of a bounding surface plasticity soil model. *Soil dynamics and earthquake engineering* **49**: 135-145, 2013.
19. Hamid TB, Miller GA. A constitutive model for unsaturated soil interfaces. *International Journal for Numerical and Analytical Methods in Geomechanics* **32**: 1693-1714, 2008.
20. Hilf JW. *An investigation of pore water pressure in compacted cohesive soils*edn: Technical Memo 654, Denver: US Bureau of Reclamation, 1956.

21. Hossain MA, Yin JH. Influence of grouting pressure on the behavior of an unsaturated soil-cement interface. *Journal of Geotechnical and Geoenvironmental Engineering, ASCE* **138**: 193-202, 2012.

22. Hu LM, Pu JL. Testing and modeling of soil-structure interface. *Journal of Geotechnical and Geoenvironmental Engineering, ASCE* **130**: 851-860, 2004.

23. Hu R, Liu H-H, Chen Y, Zhou C, Gallipoli D. A constitutive model for unsaturated soils with consideration of inter-particle bonding. *Computers and Geotechnics* **59**: 127-144, 2014.

24. Khalili N, Khabbaz MH. A unique relationship for chi for the determination of the shear strength of unsaturated soils. *Geotechnique* **48**: 681-687, 1998.

25. Khoury CN, Miller GA, Hatami K. Unsaturated soil–geotextile interface behavior. *Geotextiles and Geomembranes* **29**: 17-28, 2011.

26. Lade PV, Nelson RB. Modelling the elastic behaviour of granular materials. *International Journal for Numerical and Analytical Methods in Geomechanics* **11**: 521-542, 1987.

27. Lashkari A. On the modeling of the state dependency of granular soils. *Computers and Geotechnics* **36**: 1237-1245, 2009.

28. Lashkari A. Prediction of the shaft resistance of nondisplacement piles in sand. *International Journal for Numerical and Analytical Methods in Geomechanics* **37**: 904-931, 2013.

29. Lashkari A, Kadivar M. A constitutive model for unsaturated soil–structure interfaces. *International Journal for Numerical and Analytical Methods in Geomechanics* **40**: 207-234, 2016.

30. Lashkari A, Torkanlou E. On the constitutive modeling of partially saturated interfaces. *Computers and Geotechnics* **74**: 222-233, 2016.

31. Li XS. A sand model with state-dapendent dilatancy. *Géotechnique* **52**: 173-186, 2002.

32. Li XS, Dafalias YF. Dilatancy for cohesionless soils. *Géotechnique* **50**: 449-460, 2000.

33. Liu H, Song E, Ling HI. Constitutive modeling of soil-structure interface through the concept of critical state soil mechanics. *Mechanics Research Communications* **33**: 515-531, 2006.

34. Liu J, Zou D, Kong X. A three-dimensional state-dependent model of soil–structure interface for monotonic and cyclic loadings. *Computers and Geotechnics* **61**: 166-177, 2014.

35. Lloret-Cabot M, Wheeler SJ, Sánchez M. A unified mechanical and retention model for saturated and unsaturated soil behaviour. *Acta Geotechnica* **12**: 1-21, 2017.

36. Lloret‐Cabot M, Sánchez M, Wheeler SJ. Formulation of a three‐dimensional constitutive model for unsaturated soils incorporating mechanical–water retention couplings. *International Journal for Numerical and Analytical Methods in Geomechanics* **37**: 3008-3035, 2013.

37. Lu N, Godt JW, Wu DT. A closed‐form equation for effective stress in unsaturated soil. *Water Resources Research* **46**, 2010.

38. Ng CWW, Menzies B. *Advanced unsaturated soil mechanics and engineering*edn: Taylor & Francis, London and NY, 2007.

39. Ng CWW, Xu J, Yung SY. Effects of wetting-drying and stress ratio on anisotropic stiffness of an unsaturated soil at very small strains. *Canadian Geotechnical Journal* **46**: 1062-1076, 2009.

40. Ng CWW, Yung SY. Determination of the anisotropic shear stiffness of an unsaturated decomposed soil. *Géotechnique* **58**: 23-35, 2008.

41. Nuth M, Laloui L. Effective stress concept in unsaturated soils: Clarification and validation of a unified framework. *International journal for numerical and analytical methods in Geomechanics* **32**: 771-801, 2008.

42. Samtani NC, Desai CS, Vulliet L. An interface model to describe viscoplastic behavior.

International journal for numerical and analytical methods in geomechanics **20**: 231-252, 1996.

43. Shahrour I, Rezaie F. An elastoplastic constitutive relation for the soil-structure interface under cyclic loading. *Computers and Geotechnics* **21**: 21-39, 1997.
44. Sheng D. Non-convexity of the Barcelona Basic Model-Comment on SJ Wheeler, D. Gallipoli and M. Karstunen (2002; 26: 1561-1571). *International Journal for Numerical and Analytical Methods in Geomechanics* **27**: 879-881, 2003.
45. (2016). Thermo-mechanical hypoplastic interface model for fine-grained soils. *Proceedings of the 1st International Conference on Energy Geotechnics*. pp 351-357.
46. Terzaghi K. *Theoretical soil mechanics*edn: John Wiley and Sons, New York, NY, 1943.
47. Van Genuchten MT. A closed-form equation for predicting the hydraulic conductivity of unsaturated soils. *Soil Science Society of America journal* **44**: 892-898, 1980.
48. Wan R, Guo P. A simple constitutive model for granular soils: modified stress-dilatancy approach. *Computers and Geotechnics* **22**: 109-133, 1998.
49. Wang G, Xie Y. Modified bounding surface hypoplasticity model for sands under cyclic loading. *Journal of Engineering Mechanics* **140**: 91-101, 2014.
50. Wang Z-L, Dafalias YF, Shen C-K. Bounding surface hypoplasticity model for sand. *Journal of engineering mechanics* **116**: 983-1001, 1990.
51. Wheeler S, Gallipoli D, Karstunen M. Comments on use of the Barcelona Basic Model for unsaturated soils. *International journal for numerical and analytical methods in Geomechanics* **26**: 1561-1571, 2002.
52. Wheeler SJ, Sharma RS, Buisson MSR. Coupling of hydraulic hysteresis and stress-strain behaviour in unsaturated soils. *Géotechnique* **53**: 41-54, 2003.
53. Zhang G, Zhang J. State of the art: Mechanical behavior of soil–structure interface. *Progress in Natural Science* **19**: 1187-1196, 2009.

54. Zhou C, Ng CWW. Simulating the cyclic behaviour of unsaturated soil at various temperatures using a bounding surface model. *Geotechnique* **66**: 344-350, 2016.

55. Zhou C, Ng CWW, Chen R. A bounding surface plasticity model for unsaturated soil at small strains. *International Journal for Numerical and Analytical Methods in Geomechanics* **39**: 1141-1164, 2015.

List of figures

List of tables

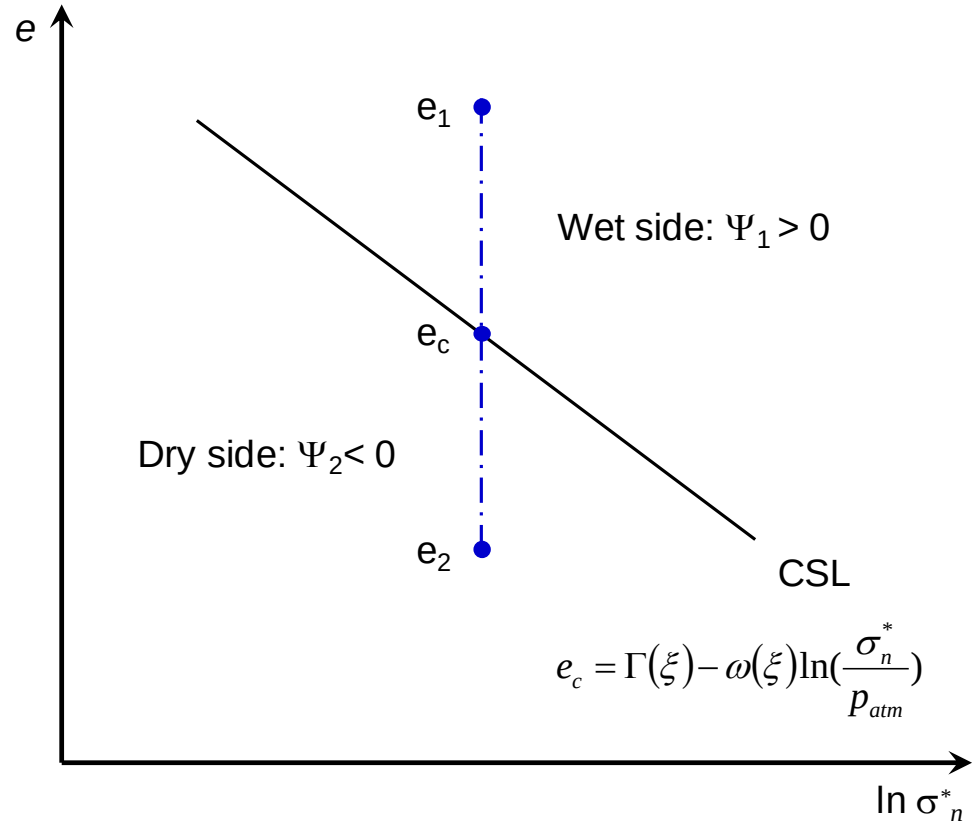

Figure 1. Definition of the state parameter ψ in equation (10)

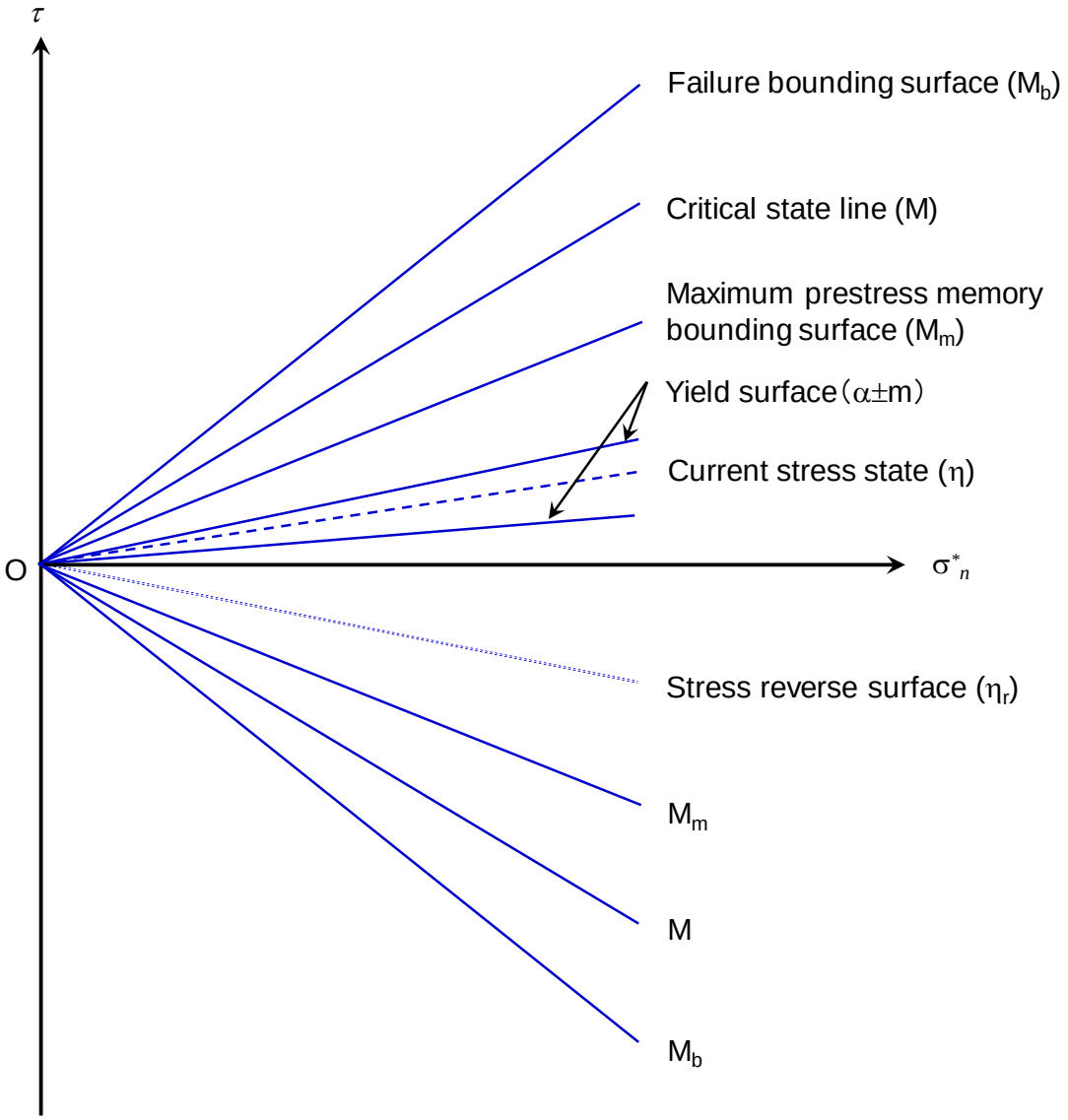

Figure 2. Schematic of two bounding surfaces and one yield surface

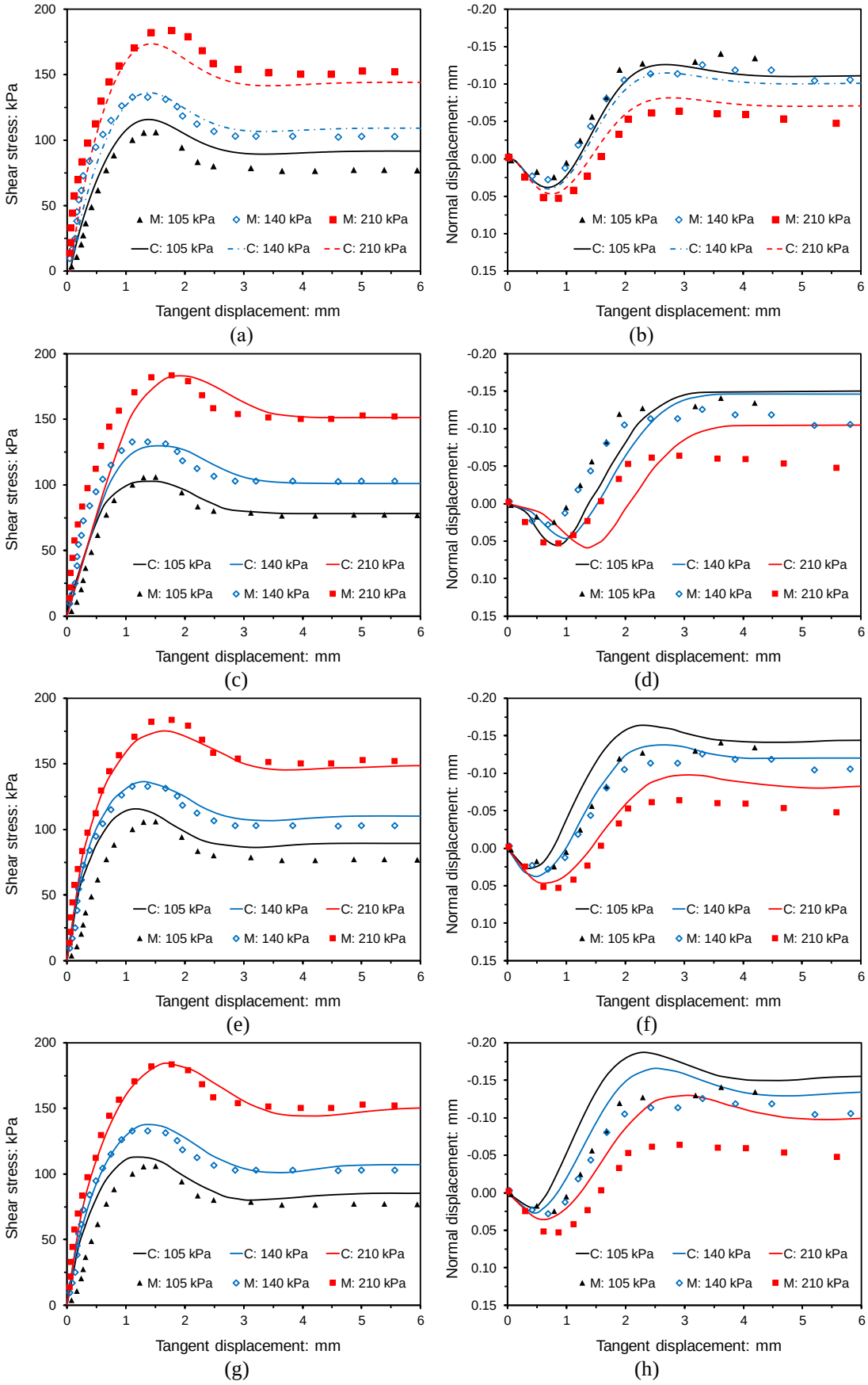

Figure 3. Comparisons between measured [19] and computed behaviour of a soil-steel interface at a suction of 100 kPa and various net stresses: (a)-(b): the current model; (c)-(d) model of Hamid et al. [19]; (e)-(f) model of Lashkari et al. [29]; (g)-(h) model II of Lashkari et al. [30]

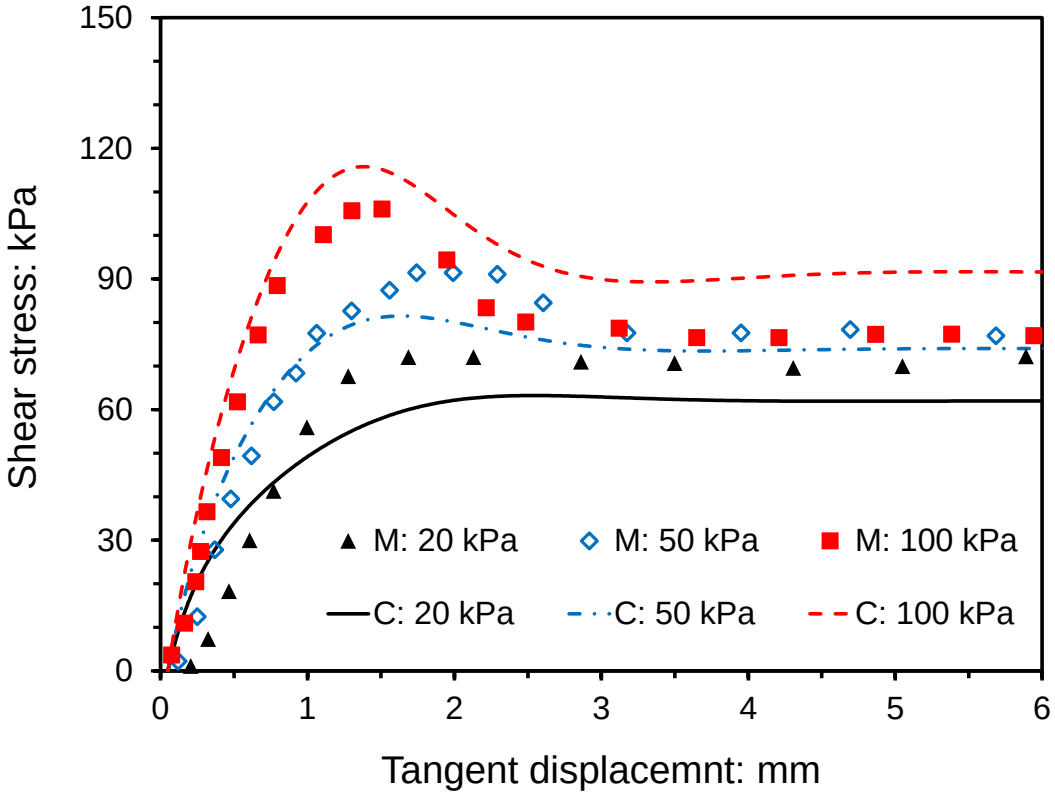

(a)

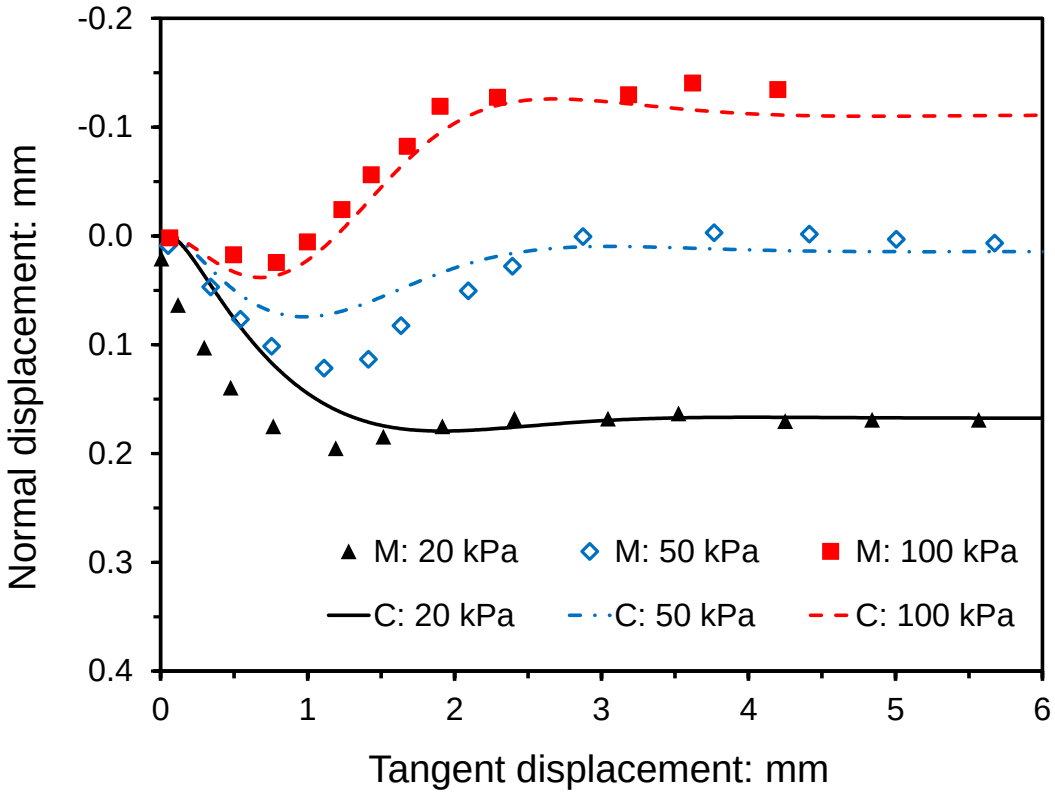

(b)

Figure 4. Comparisons between measured (M) [19] and computed (C) shear behaviour of an soil- steel interface at net normal stress of 105 kPa and various suctions

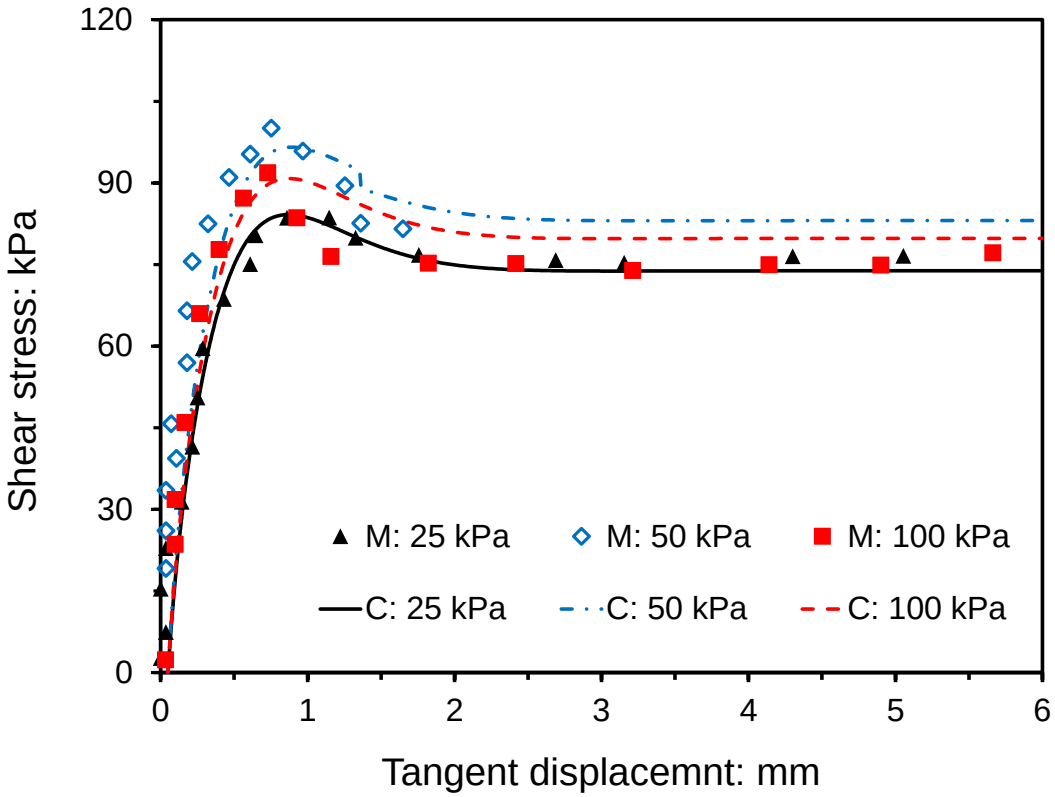

(a)

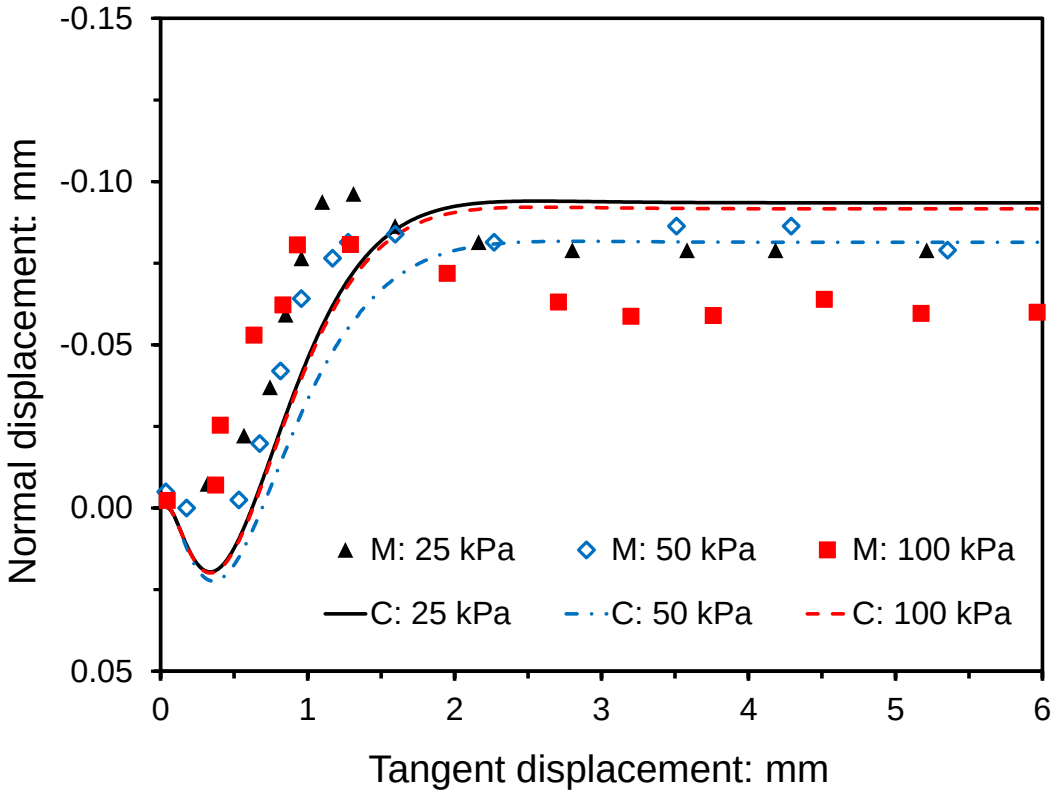

(b)

Figure 5. Comparisons between measured [25] and computed shear behaviour of a soil-geotextile interface at net normal stress of 100 kPa and various suctions

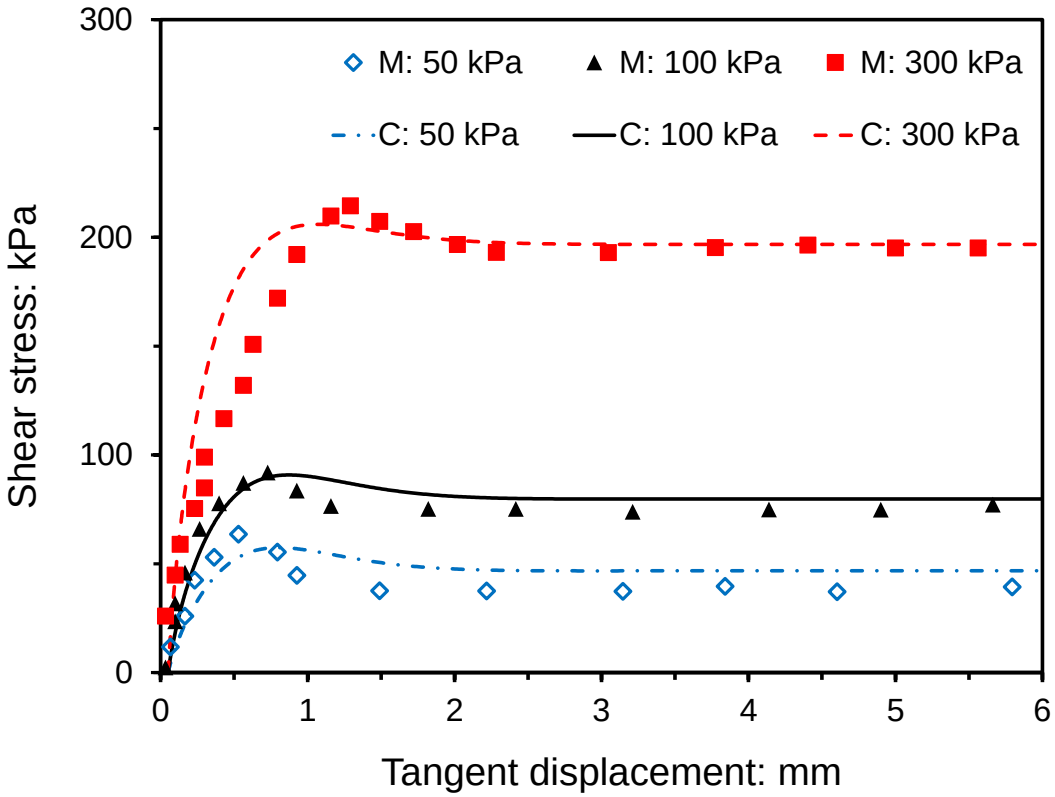

(a)

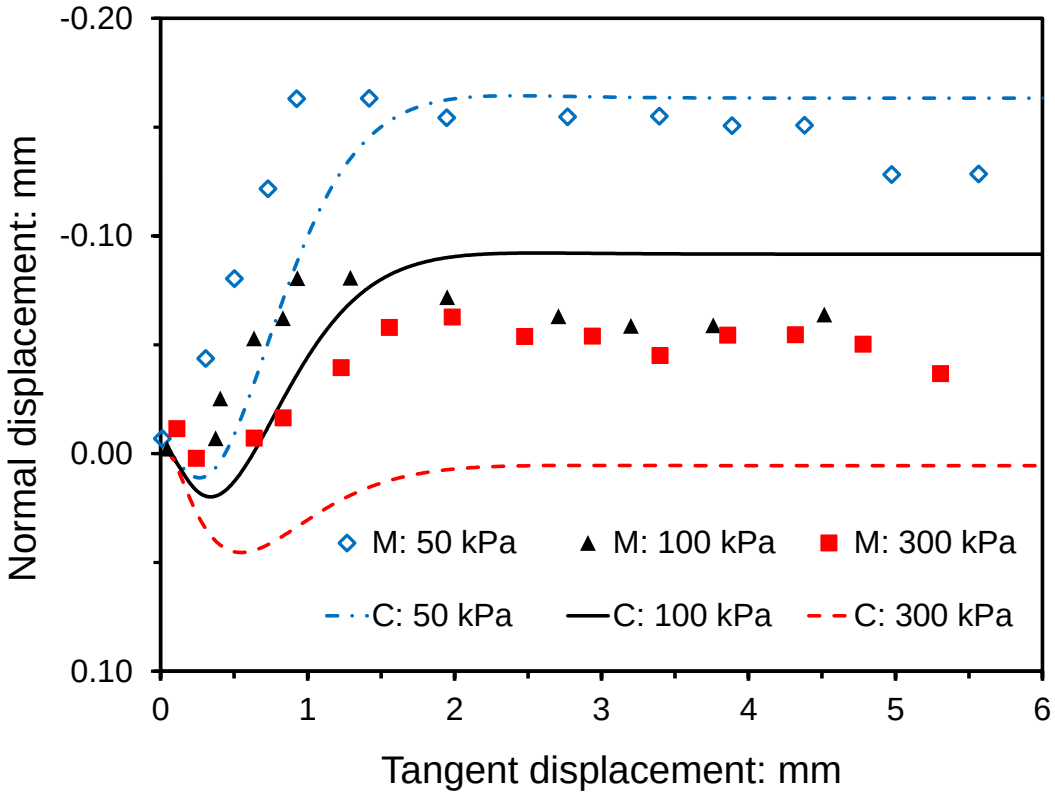

(b)

Figure 6. Comparisons between measured [25] and computed shear behaviour of a soil-geotextile interface at a suction of 100 kPa and various normal stresses

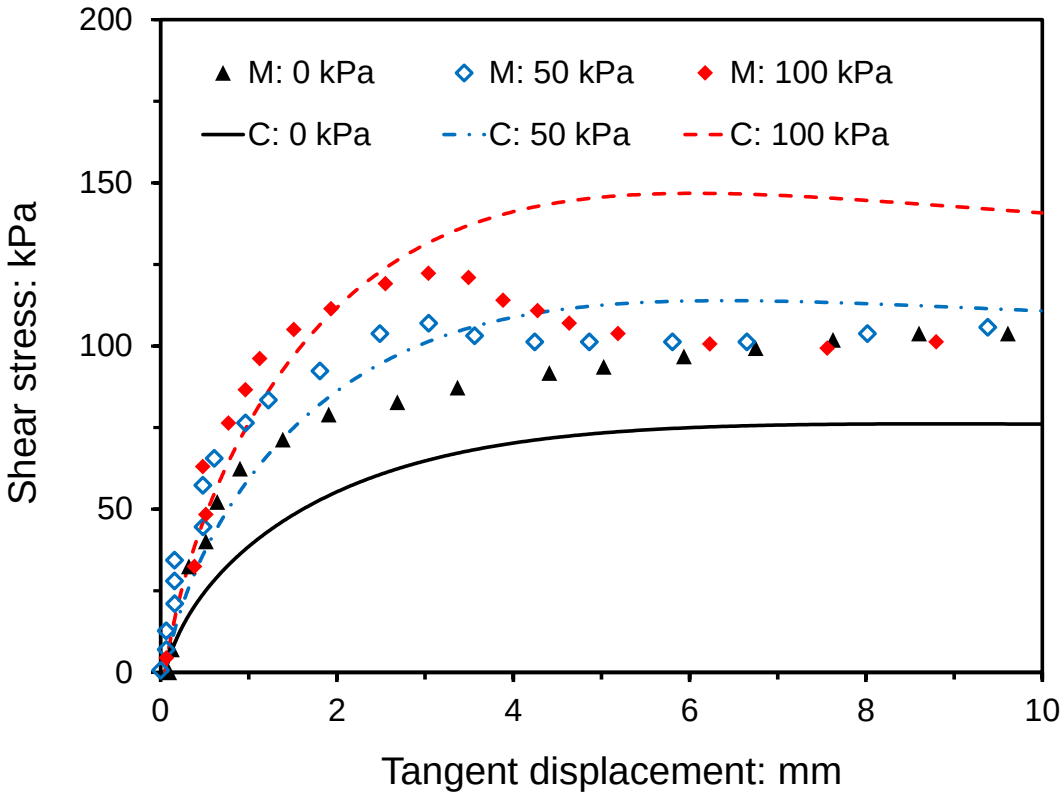

(a)

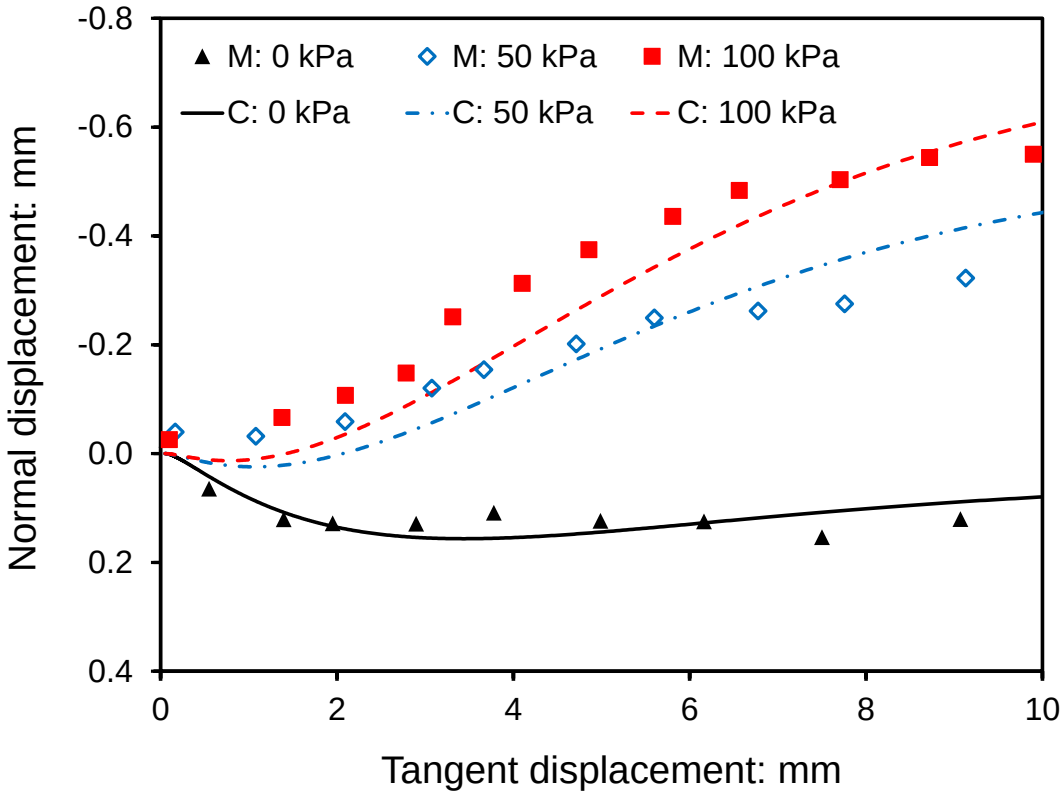

(b)

Figure 7. Comparisons between measured [21] and computed shear behaviour of a soil-cement interface at net normal stress of 100 kPa and various suctions

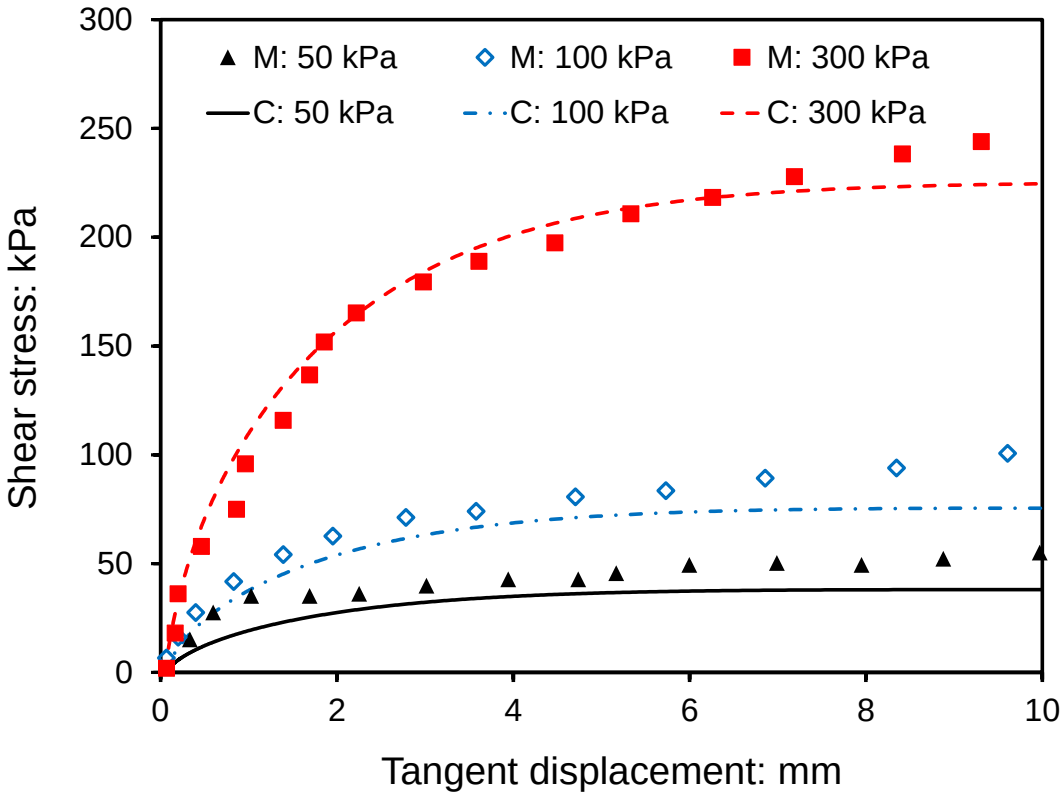

(a)

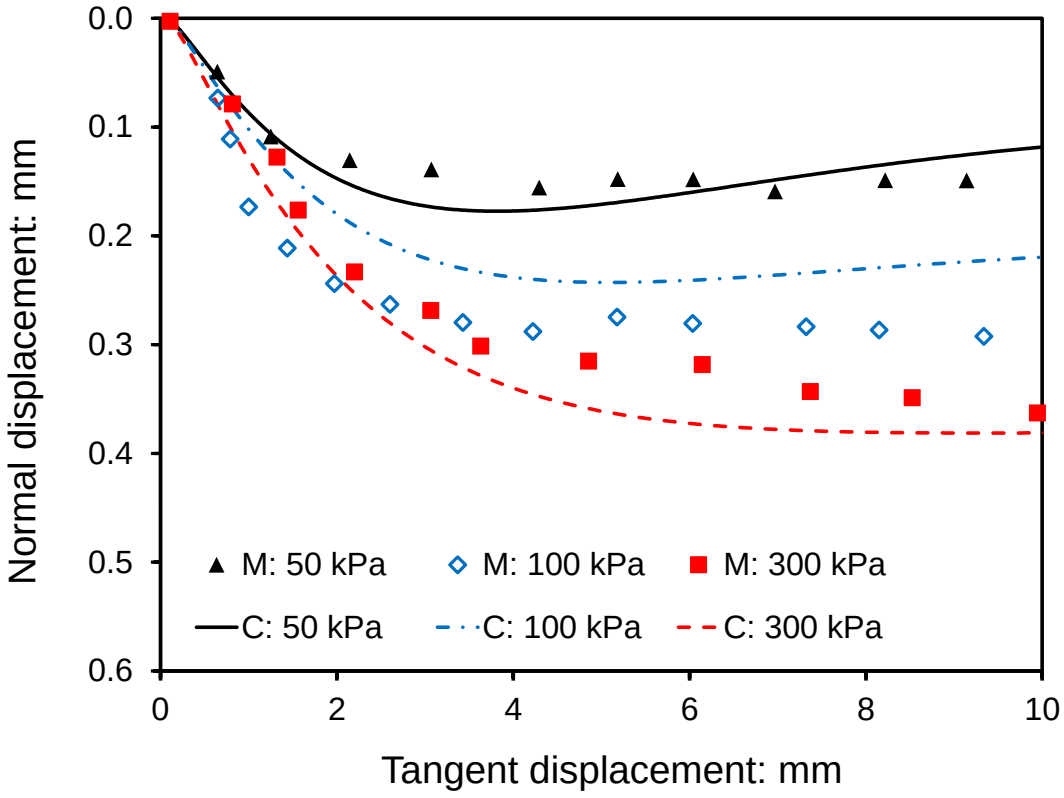

(b)

Figure 8. Comparisons between measured [21] and computed shear behaviour of a soil- cement interface at zero suction and various effective normal stresses

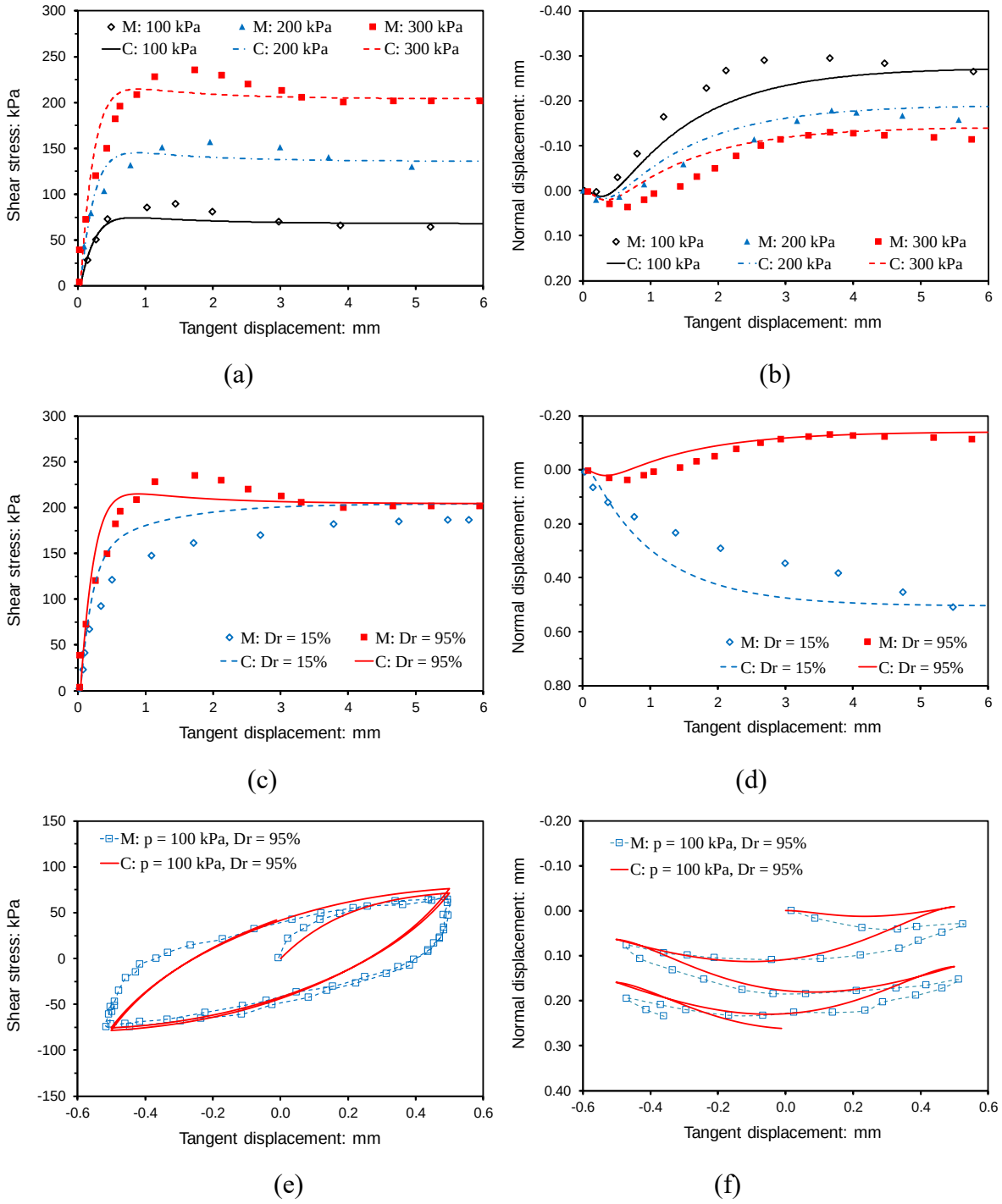

Figure 9. Monotonic and cyclic shear behaviour of a sand-steel interface tested by Shahrour *et al.* [43] at saturated condition: (a)-(b) Dr = 95%; (c)-(d) effective normal stress of 100 kPa; (e)-(f) cyclic shear behaviour

Table I. Summary of model parameters and their values for various soil-structure interfaces

Soil parameters		Soil-steel interface [19]	Soil-geotextile interface [25]	Soil-cement interface [21]	Sand-steel interface [43]
Water retention behaviour	m_1	1	0.5	1	NIL*
	m_2	1	2.5	0.8	NIL*
	m_3 (kPa)	400	20	200	NIL*
Interface thickness	t (mm)	5	5	5	5
Elastic property	D_{t0} (kPa)	250	700	200	800
	R	2	3	4	1
Critical state line	M	0.5	0.6	0.75	0.68
	Γ_s	0.625	0.75	0.52	0.8
	ω_s	0.03	0.04	0.05	0.07
	a	2	0.05	1.5	NIL*
	b	0.5	0.1	1.5	NIL*
Flow rule	d_0	0.5	0.5	0.2	0.32
	n_d	1	5	3	0.8
Hardening law	h	0.8	0.5	0.2	1
	n_b	8	6	1	1

Note: * These parameters are not necessary in simulating saturated interfaces.

Table II. Parameter values used by models for a soil-steel interface tested by Hamid *et al.* [19]

Model	Model of Hamid *et al.* [19]	Model of Lashkari *et al.* [29]	Model II of Lashkari *et al.* [30]
Parameters and their values	$K_r^e = 300\ kPa$	$K_n = 1000\ kPa$	$K_r^e = 281\ kPa$
	$K_n^e = 310\ kPa$	$K_s = 150\ kPa$	$K_n^e = 292\ kPa$
	$M = 0.54$	$n\ = 4$	$M = 0.62$
	$e_0 = 0.125$	$a = 17.4$	$\Gamma_0 = 0.346$
	$\lambda = 0.145$	$b = 2.85$	$\lambda_0 = 0.081$
	$n^b = 3$	$\xi_{D1} = 0.0318\ mm$	$a = 145$
	$n^d = 1.2$	$\xi_{D2} = 0.0951\ mm$	$b = 1.336$
	$A_0 = 0.65$	$\mu_{p1}\ = 0.2796$	$A_0 = 0.65$
	$A_1 = 0.65$	$\mu_{p2}\ = 0.0635$	$A_1 = 0.40$
	$h_0 = 0.4$	$\mu_{01}\ = 0.3479$	$h_0 = 0.32$
	$a = 25$	$\mu_{02}\ = 0.049$	$n = 2.5$
	$b = 4.3$	$\kappa_1\ = 0.4728$	$m = 0.8$
	$S_{r0} = 0.2$	$\kappa_2\ = -0.0316$	$S_{r0} = 0.2$
	$\alpha_w = 0.104$	$\lambda_{(s)}\ = 0.399$	$\theta = 1.6$
	$n_v = 1.275$	$\lambda_1\ = -5.2285$	$\alpha_w = 0.1045$
	$\Omega = 1.6$	$\lambda_2\ = 29.4865$	$n_v = 1.275$
			$s_{ae} = 13\ kPa$